TRANSACTIONS OF THE INSTITUTE OF FLUID-FLOW MACHINERY

No. 138, 2017, 13–32

Kamil Banaś* and Janusz Badur

Effect of turbulence model, turbulence length scale and wall roughness on the laminar-turbulence transition and temperature distribution of a convectively cooled C3X turbine vane

Department of Energy Conversion Institute of Fluid Flow Machinery, Polish Academy of Sciences 80-231 Gdansk, Fiszera 14, Poland

Abstract

Our paper demonstrates the ability of Favre-averaged Navier–Stokes (FANS) turbulence models to predict the laminar-turbulent transition and shows the influence of the models on the wall temperature distribution. The investigations were based on conjugate heat transfer analyses of a convectively cooled C3X turbine vane, which were performed using commercial flow simulation software. We compared several eddy-viscosity models: shear stress transport (SST), γ-Re$_\theta$ SST-transition, v^2-f, k-ε, realizable, k-kl-ω transition, and second-order closure ε-based Reynolds stress model (RSM) with a linear pressure-strain model. The turbulence length scale (TLS) was not measured during the experiment, so its influence on the location of the transition onset and wall temperature distribution is presented. We also examined the influence of the roughness of the airfoil wall on the location of turbulence initialization and the wall temperature distribution.

Keywords: Laminar-turbulent transition; Conjugate heat transfer analysis of turbine; C3X turbine vane; Roughness correction

1 Introduction

The inlet temperature plays an essential role in the performance of gas and steam turbines, where cyclic thermo-elasto-plasticity and high-temperature creep may interact and contribute to failure [1–3]. Much effort has been made to develop

*Corresponding Author. Email adress: kbanas@imp.gda.pl

methods to predict the temperature, thermal stresses, and associated lifetime of critical components in the aerospace and power generation industries [4–10]. Accurate evaluation of the temperature distribution is important for these processes, and the turbulence model has an important influence on that.

It is common knowledge that none of the Reynolds/Favre-averaged Navier–Stokes (RANS/FANS) turbulence models can capture all the effects in a flow, such as transitions, secondary flows, and separations. Strong inhomogeneity and anisotropy appear in the near-wall region [11,12]. This region is therefore very demanding for RANS/FANS models, which provide a statistical description of the turbulent flows. Moreover, for turbine blades, a transition from laminar to turbulent flow in the boundary layer very often appears, which strongly influences the heat transfer on the airfoil.

> *Can turbulence models describe transition from laminar to turbulent flow? They are developed for fully turbulent conditions and calibrated with turbulence data; the answer would seem to be 'no.' However, most transport equation models do converge to a laminar solution at low Reynolds number and to a turbulent solution at sufficiently high Reynolds number; the model equations do evidence a transition between laminar and turbulent solution branches.*
>
> P. A. Durbin and B. A. Pettersson Reif [12]

RANS/FANS models such as the Spalart–Allmars (S–A), k-ε, k-ω, and SST work as 'fully-turbulent' models or create an apparent transition point, which does not correlate with experiments [13,14]. However, more advanced RANS/FANS turbulence models such as the v^2-f or RSM take into account anisotropy of the Reynolds stresses in the near-flow region, and they are very often able to capture the laminar-turbulent transition in the boundary layer [15–17]. Durbin and Pettersson Reif [12] claim that turbulence models obtain length scales from a transport equation, which influences their ability to emulate a transition. However, the precise mathematical origin of that capability is not well understood. They explain that this behaviour is a property of the model equations, not of fluid dynamical mechanisms. Therefore, when accurate predictions of the laminar and transitional regions are needed, the turbulence model must be supplemented explicitly by a method to predict the transition.

One of the most promising approaches to control all types of transitions is the γ-Re$_\theta$ transition model proposed by Menter *et al.* [18]. The γ-Re$_\theta$ transition model is experimental correlation based model. This model uses two transport

equations: one for the intermittency, γ, and one for the transition onset of the momentum-thickness Reynolds number, $\mathrm{Re}_{\theta t}$. The intermittency represents the fraction of time that the flow is turbulent, which is 0 in the laminar boundary layer and 1 in the fully turbulent layer. The intermittency transport equation is used to trigger the transition onset and to model the transition region. The $\mathrm{Re}_{\theta t}$ is used as a criterion for the location of the transition onset. The transport equation for $\mathrm{Re}_{\theta t}$ is used for avoiding non-local operations introduced by experimental correlations. The γ-Re_{θ} transition model coupled with the SST model [18] enables the prediction of different kinds of transitions [19–22].

Our paper demonstrates the ability of FANS turbulence models to predict the laminar-turbulent transition and shows the influence of the models on the wall temperature distribution. Our investigation is based on a convectively cooled C3X turbine vane, which was extensively tested by Hylton *et al.* [23]. We compared several eddy-viscosity models: the SST, γ-Re_{θ} SST-transition, v^2-f, k-ε, realizable, k-kl-ω transition, and second-order closure ε-based RSM with a linear pressure-strain model. The investigation was based on conjugate heat transfer analyses. The Favre-averaged compressible Navier–Stokes equations were resolved using ANSYS Fluent software.

Hylton and co-authors did not measure the turbulence length scale (TLS) during his experiments, which has a significant influence on the laminar turbulent transition and heat transfer [16,24]. Some guidelines are available about the size of the largest energy-containing eddies in ducts. However, experiments of Hylton and co-authors used turbulence-augmenting rods to maintain an assumed value of the turbulence intensity, Fig. 1. The influence of TLS on the location of the transition onset and heat transfer has been presented previously [16,24], but those studies did not consider several models simultaneously. Therefore, we investigated the influence of TLS on the results produced by models that can capture the laminar-turbulent transition.

Moreover, Hylton and co-authors did not provide information about the roughness of the airfoil wall, which influences the location of the transition onset and the heat transfer in the turbulent boundary layer by disturbing or destroying the viscous sublayer. Therefore, we examined influence of the wall roughness on the results of the γ-Re_{θ} SST-transition model. The model engages two types of roughness. One is the geometric roughness, which is involved in the intermittency transport equation and influences the location of the transition onset. The second type of roughness is the 'sand grain' roughness, which produces additional shear stress in the turbulent boundary layer. During the investigation of the roughness effects on the transition location, we considered a few typical values of

wall roughness produced by grinding according to the definition of the ten-point mean roughness, R_z, which is a more accurate representation of roughness for computational fluid dynamics (CFD) analysis [25].

2 Test case description

Hylton and co-authors conducted a series of heat transfer experiments with a C3X turbine vane. A cascade consisting of three vanes was considered to provide periodicity to the flow, Fig. 1. The experimental approach employed a 2-D model technique, so a constant cross section was applied to the vane and the 2-D properties of the flow were checked by additional measurements [23]. A detailed geometry description is available elsewhere [23].

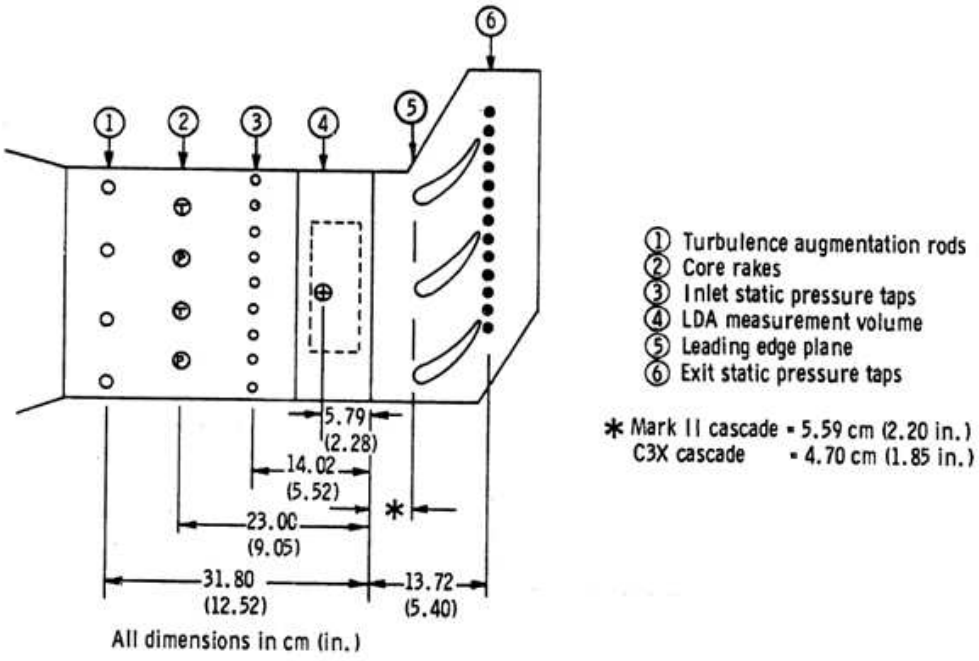

Figure 1: C3X cascade dimensions and location of instrumentation.

Test case no. 4311 was chosen for the numerical investigations. Table 1 presents the measured quantities of the main flow used as the boundary conditions, including the total inlet temperature, total inlet pressure, inlet turbulence intensity, and outlet static pressure.

Table 1: Boundary conditions.

Test case	Inlet total temperature, K	Inlet total pressure, Pa	Outlet pressure, Pa	Turbulence intensity, %
4311	802	244764	143000	6.5

The vane was cooled by an array of 10 radial cooling holes. The flows in the cooling holes are simple pipe flows, for which empirical correlations for convective heat transfer are accurate enough to predict the heat transfer performance [20,26]. Based on the Nusselt number, the heat transfer coefficients were evaluated, Tab. 2, coupled with the bulk temperature of the fluid holes, and imposed as the third thermal type of boundary condition to the wall of the cooling channel. The Nusselt number for turbulent flow in a smooth pipe is represented by the following empirical formula [23]:

$$\mathrm{Nu}_D = \mathrm{Cr}(0.022\mathrm{Pr}^{0.5}\mathrm{Re}_\mathrm{D}^{0.8}) \,, \tag{1}$$

where Cr is a correction of the Nu expression for a fully developed thermal boundary layer to account for effects of the thermal entrance region [23]. The Prandtl number equal to 0.7 was used [17]. The quantities necessary to evaluate the Nusselt number for each hole are provided elsewhere [23], and the detailed boundary conditions for the cooling holes are shown in Tab. 2.

3 Conjugate heat transfer analysis

A conjugate heat transfer analyses were carried out. The Favre-averaged compressible Navier–Stokes equations were resolved using commercial CFD software, based on control volume technique, which employ the division of the domain into discrete control volumes applying computational grid. We used several eddy-viscosity models as the turbulence models: the SST, γ-Re_θ SST-transition, v^2-f, k-ε realizable, k-kl-ω transition, and second-order closure ε-based RSM with a linear pressure-strain model. A curvature correction was included in the eddy viscosity models. The pressure-coupled solver was employed with first-order upwind discretization schemes.

The numerical simulations were carried out for a 2-D case. An inlet to the fluid domain was established in the location where the turbulence intensity was measured, while the outlet was applied where the outflow parameters were aligned

Table 2: Cooling holes heat transfer coefficient (HTC) data.

Hole No.	Diameter, m	Cr	Temperature, K	Re	Nu	k, $\frac{W}{mK}$	HTC, $\frac{W}{m^2K}$
1	0.0063	1.118	360.63	154940	292	0.030729	1425
2	0.0063	1.118	360.63	161620	302	0.030729	1474
3	0.0063	1.118	346.23	159740	299	0.029675	1410
4	0.0063	1.118	352.50	158770	298	0.030136	1425
5	0.0063	1.118	341.41	170710	316	0.029319	1469
6	0.0063	1.118	380.08	161580	302	0.032132	1541
7	0.0063	1.118	352.47	162340	303	0.030134	1450
8	0.0031	1.056	387.16	104340	201	0.032637	2117
9	0.0031	1.056	421.81	63960	136	0.035063	1538
10	0.00198	1.025	466.79	46850	103	0.038107	1980

and as close as possible to where the pressure outlet was measured, Fig.1. A fine structured mesh with a conformal solid-fluid interface was created, Fig. 2. After a mesh independence study, the mesh consisted of 255 736 hex elements. Low-Reynolds turbulence models were used to capture the effects in the momentum and thermal boundary layers. The mesh was built based on the dimensionless parameter $y^+ \approx 1$ near the walls and a growth ratio below 1.1 in the boundary layer.

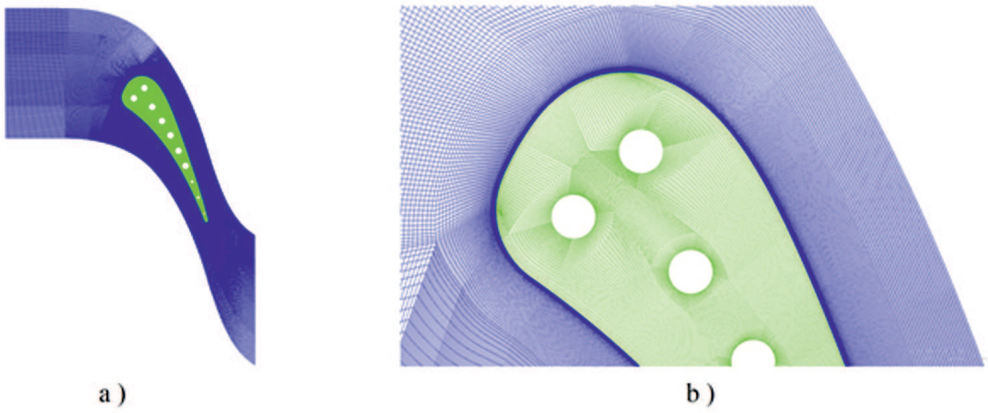

Figure 2: CFD model: a) general view, b) detail view.

The fluid domain was modelled as air with the assumption of a compressible, calorically imperfect gas. Therefore, the specific heat and other properties vary with temperature. The viscosity was obtained from Sutherland's relation [27]. The turbine material is ASTM 310 stainless steel, and the thermal conductivity k_S is specified based on the experimental data of Goldsmith et al. [28]:

$$k_S(\mathrm{T}) = 6.811 + 0.020176\,\mathrm{T}\ , \tag{2}$$

where T is temperature.

The TLS was not measured during the experiment, so we investigated its influence on the location of the transition onset and the temperature distribution. The investigation was based on three turbulence models (γ-Re_θ SST-transition, v^2-f, and RSM). The vane height is 76.2 mm, and the true chord is 144.93 mm. We assumed inlet TLSs of 2, 5, 10, and 20% of the vane height and 20% of the chord length, which correspond to TLS values of 1.52, 3.81, 7.62, 15.24, and 28.986 mm, respectively. Additionally, we determined the influence of the surface roughness on the location of the transition onset and the temperature distribution. The definition of the ten-point mean roughness, R_z, was assumed, and typical values of surface roughness for finishing grinding were considered (1.6, 3.2, and 6.3 μm).

4 Results

Figure 3 shows the typical temperature distribution for the fluid region and for the solid body of the vane for case no. 4311. The hottest region occurs at the trailing edge.

Case no. 4311 shows a mild pressure distribution, Fig. 4. The pressure distributions from the numerical analysis show good agreement with the experimental data. On the suction side near the leading edge the flow is locally supersonic, Fig. 5. After that, the bypass laminar-turbulent transition is occurred at approximately $x/L \approx 0.4$, Fig. 6. The pressure side for the γ-Re$_\theta$ SST-transition model is captured by the laminar boundary layer, Fig. 6.

4.1 Influence of the turbulence model on transition prediction

The influence of the turbulence models on the prediction of the laminar-turbulent transition was examined. For this purpose, we assumed a hydraulically smooth surface and a TLS equal to 15.24 mm. Figure 7 shows the distribution of the heat transfer coefficient (HTC) for different turbulence models along the suction and

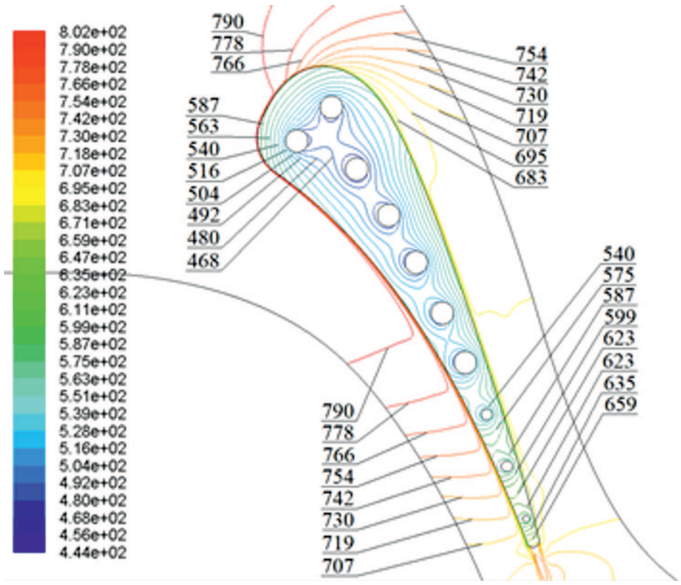

Figure 3: Temperature distribution for SST-transition turbulence model for TLS of 15.24 mm.

pressure side, which is defined as follows:

$$\mathrm{HTC} = \frac{\mathrm{q}}{\mathrm{T_{wall}} - \mathrm{T_{bulk}}}\,, \tag{3}$$

where the bulk temperature T_{bulk} was assumed to be 811 K [22], T_{wall} denotes temperature of the wall, and q is the local heat flux.

Figure 8 shows the wall temperature distribution for different turbulence models. Comparison of Figs. 7 and 8 indicates that the increase of HTC on the suction side at the location of the laminar-turbulent transition onset corresponds to a temperature rise at that point. Therefore, our investigation is based on the temperature distribution diagrams. Figure 8 shows that three models can capture the transition phenomena, namely γ-Re_θ SST-Transition, v^2-f, and RSM. Whereas, the SST and k-ε Realizable models do not capture this effect. The figure also shows that the turbulence part of the boundary layer on the suction side is more accurately described by the 'fully turbulent' models SST and k-ε realizable than by the γ-Re_θ SST-transition model. The v^2-f model and RSM also capture this region very well. The k-ε realizable model significantly over-predicts the temperature at the stagnation point.

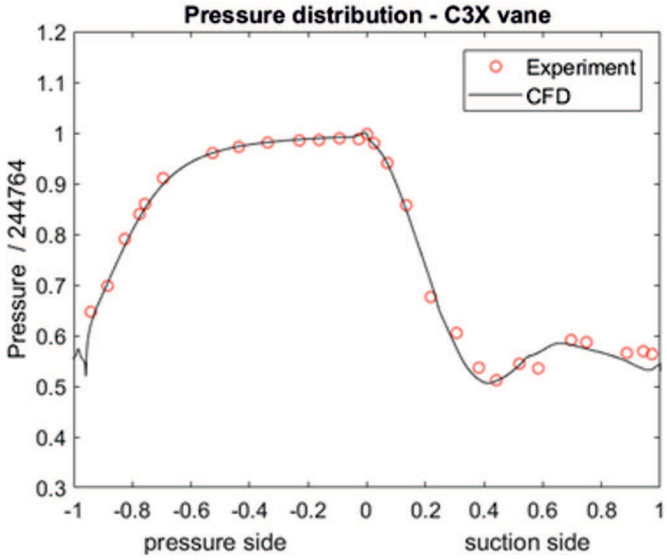

Figure 4: Pressure distribution for SST-transition turbulence model for TLS of 15.24 mm.

4.2 Influence of the turbulence length scale

Figure 8 shows that the γ-Re$_\theta$ SST-transition model, v^2-f model, and RSM can capture the laminar turbulent transition, but they produce different temperature values. The TLS was not measured during the experiment, so we investigated its influence on the accuracy of the results. Figures 9–12 show that TLS significantly influences the temperature predicted by the models, especially in the laminar zone. Moreover, the location of the transition onset depends on TLS for the γ-Re$_\theta$ SST-transition and RSM linear models, while the v^2-f model shows a constant location of the turbulence initiation.

For all considered models, the temperature distribution increased when TLS increased. For the v^2-f model and RSM, the results are most accurate for relatively small TLS values of 1.524 and 3.81 mm. The γ-Re$_\theta$ SST-transition model showed the opposite trend and is more accurate for higher TLS values of 15.24 mm. The reason of this can be application of a production limiter in SST-transition model. In Fig. 10 we see, that results obtained using SST-transition model without limiter show similar trends to results evaluated by v^2-f and RSM models. For a TLS of 1.524 mm, the γ-Re$_\theta$ SST-transition model did not predict the laminar-turbulent transition, Fig. 9.

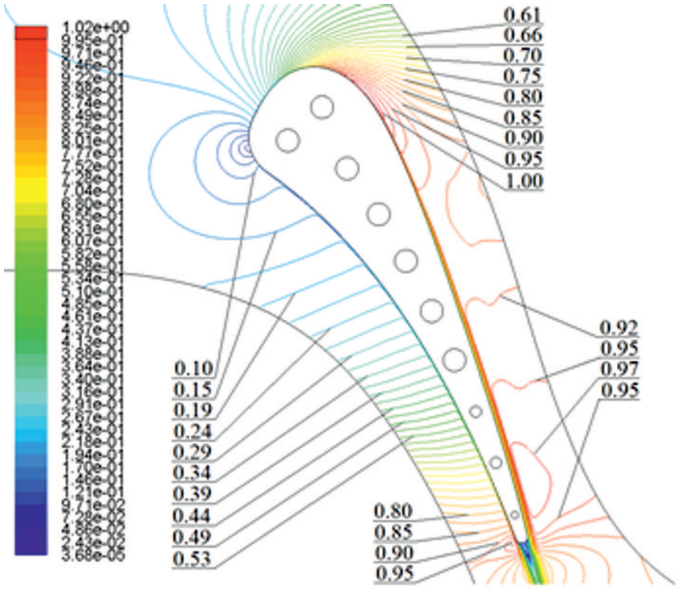

Figure 5: Contour of Mach number for the SST-transition model for TLS of 15.42 mm.

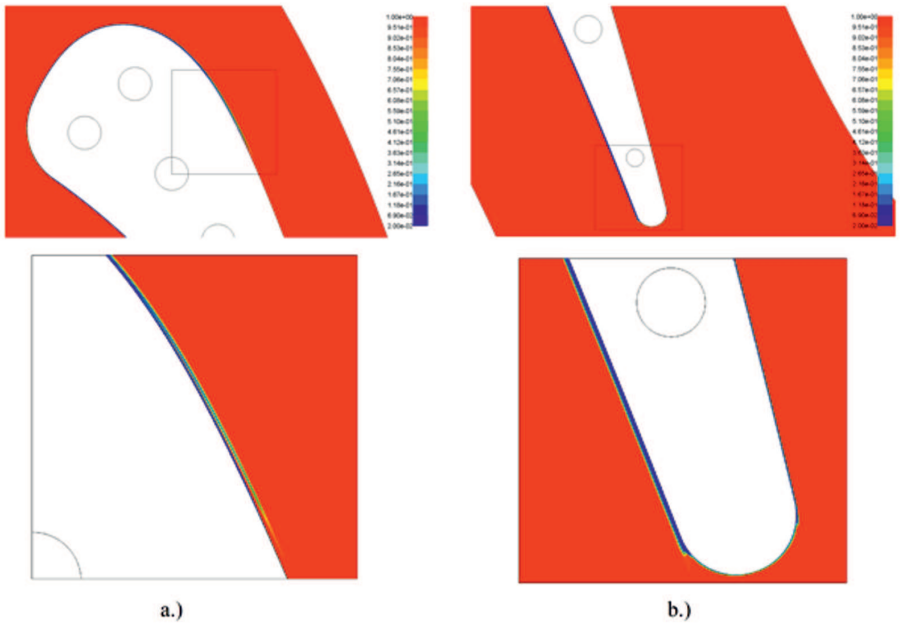

Figure 6: Intermittency distribution for the SST-transition model for TLS of 15.42 mm in areas of a) the leading edge and b) trailing edge.

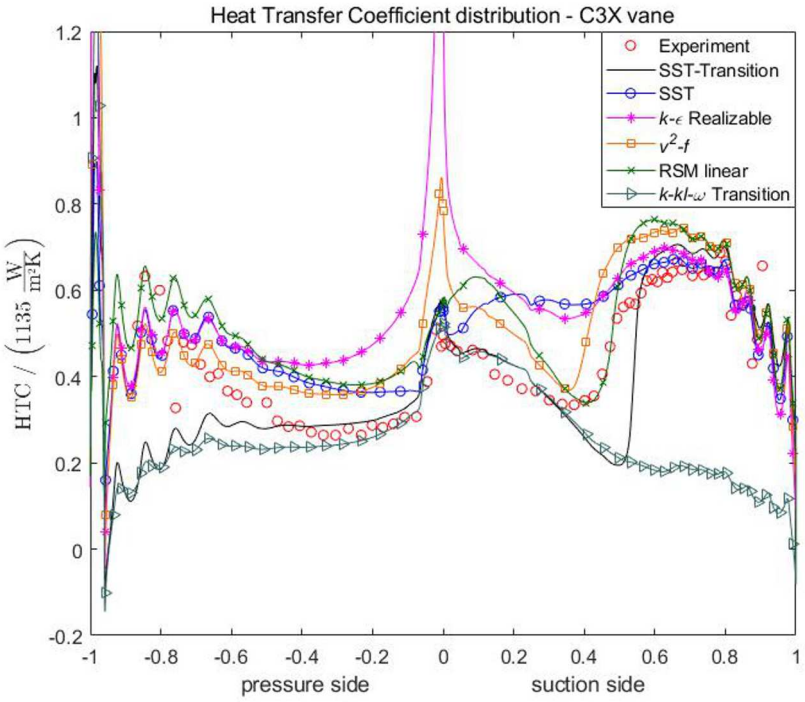

Figure 7: HTC distribution for different turbulence models for TLS of 15.24 mm.

4.3 Influence of wall roughness

The wall roughness is another parameter that was not provided but influences the near-wall region. Based on the γ-Re$_\theta$ SST-transition model and assuming a TLS of 15.24, we investigated the influence of the wall roughness on the location of the transition onset and the temperature distribution. For the γ-Re_θ SST-transition model, we applied two types of roughness: the geometric roughness and the sand grain roughness. The sand grain roughness is used to increase the wall shear stress and break up the viscous sublayer in the turbulent boundary layer. The roughness correlation used in the transport intermittency equation influences the location of the transition onset.

4.3.1 The roughness correction of laminar-turbulent transition process

The roughness correlation used in the γ-Re$_\theta$ SST-transition model requires the geometric roughness height K as an input parameter since it is more important

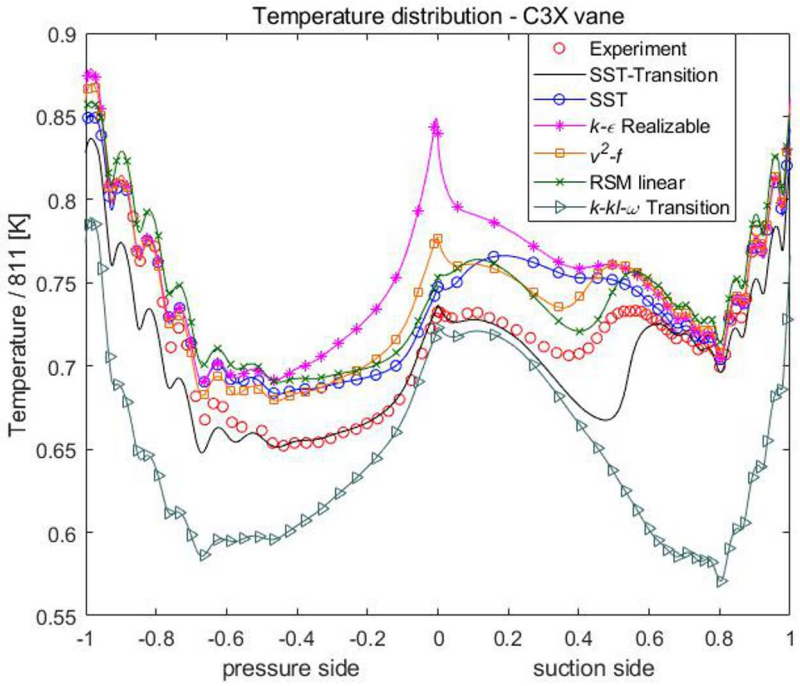

Figure 8: Temperature distribution for different turbulence models for TLS of 15.24 mm.

than the equivalent sand-grain roughness height K_S for the transition process from laminar to turbulent flow [29]. The geometric roughness height influences the correlations for the location of the transition onset and the length of the transition zone [29]. Figure 13 shows the temperature distribution for a smooth surface and for three surface-roughness parameters: 1.6, 3.2, and 6.3 μm. The diagram shows that higher wall roughness leads to the location of the transition onset moving upstream. Moreover, for a wall roughness of 6.3 μm, a bypass transition occurred on the pressure side, as shown in Figs. 14 and 15. This eventually leads to a higher temperature in the solid body, Fig. 13.

4.3.2 The roughness correction of turbulent boundary layer

The addition of roughness sensitivity to the turbulent eddy viscosity is the most common approach to enhance the turbulence in the near-wall region caused by a rough wall when using low-Reynolds eddy viscosity turbulence models [30–31]. This is predominantly applied by including a correction for the roughness in the

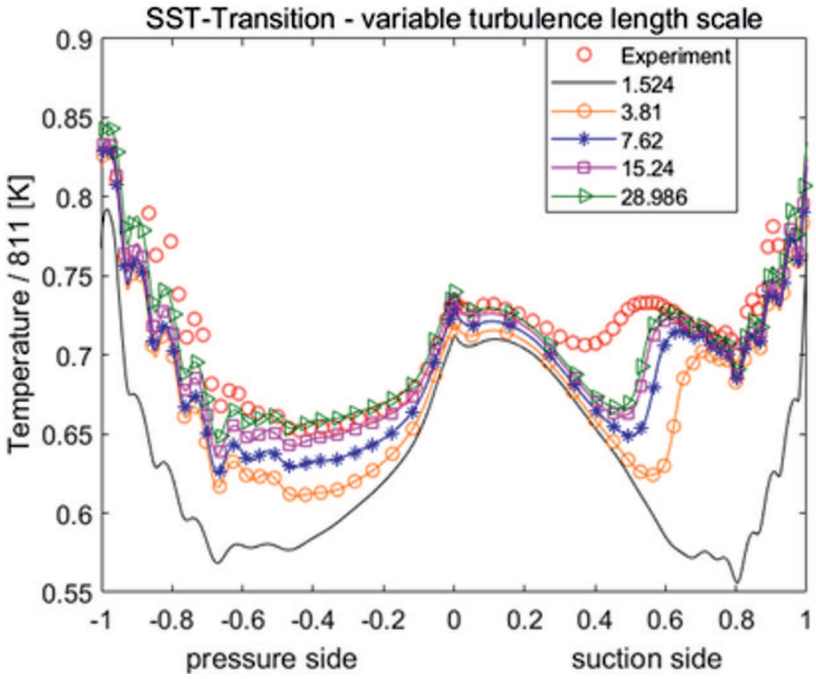

Figure 9: Temperature distribution for SST-transition turbulence model for different TLS.

turbulence quantities, such as the specific turbulence dissipation or kinetic energy. A majority of corrections based on the sand grain roughness value, which can be evaluated from following relation [32]:

$$K_S = 0.978 R_Z \ , \tag{4}$$

where R_Z is the real wall roughness based on the ten-point mean roughness definition.

Experiments indicate that the mean velocity distribution near rough walls has the same slope but a different intercept when plotted on the usual semi-logarithmic scale. Therefore, the velocity profile is shifted downward when the wall roughness appears. The downward shift leads to a singularity for large roughness heights and low values of y^+. To avoid this singularity, the application of the sand grain roughness coupled with the low-Reynolds turbulence model requires to a virtual shift of the wall to 50% of the height of the roughness elements. This results in a corrected value for the first cell centre:

$$y^+ = y^+ + \frac{K_S^+}{2} \ . \tag{5}$$

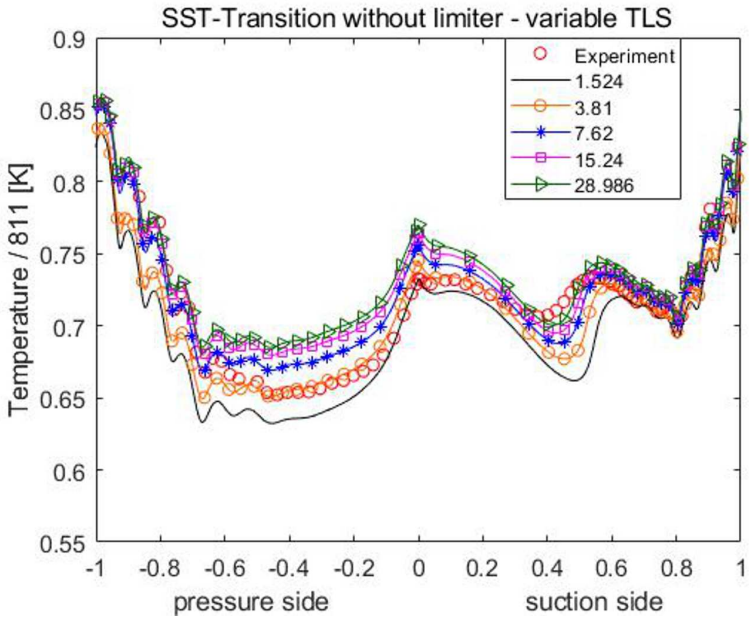

Figure 10: Temperature distribution for SST-transition turbulence model without production limiter for different TLS.

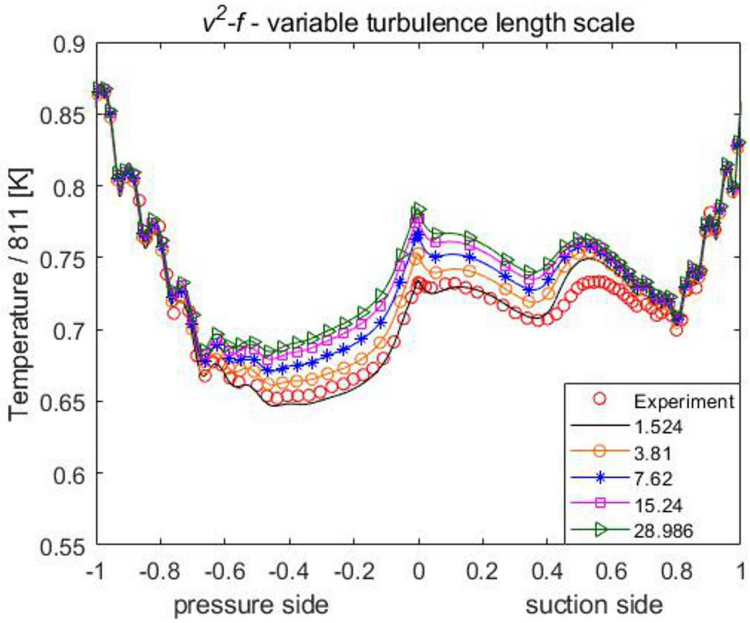

Figure 11: Temperature distribution for v^2-$f$turbulence model for different TLS.

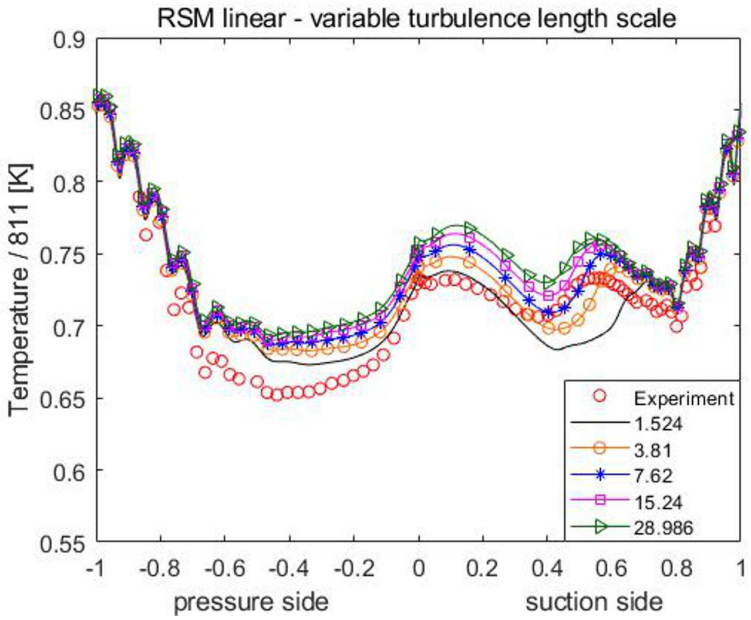

Figure 12: Temperature distribution for RSM turbulence model for different TLS.

Theoretically, the shift in the wall distance is applied to the turbulent boundary layer. However, when the γ-Re$_\theta$ SST-transition model is used, the shift is also applied to the laminar zone. This affects the temperature distribution in the laminar zone, as shown in Fig. 16. The figure shows that disturbing the viscous sublayer significantly influences the heat transfer in the turbulent zone.

5 Conclusion

Our paper has demonstrated the ability of FANS turbulence models to predict the laminar-turbulent transition, as well as the influence of the models on the temperature distribution in a solid body. We compared several models, among which three were able to capture the laminar-turbulent transition phenomena: the γ-Re$_\theta$ SST-transition, v^2-f, and RSM. The TLS and wall roughness were not measured during the experiment, so we investigated their influence on the location of the transition onset and the temperature distribution. The investigation of TLS was carried out based on the γ-Re$_\theta$ SST-transition, v^2-f, and RSM turbulence models, while that of the wall roughness was based on the γ-Re$_\theta$ SST-transition model.

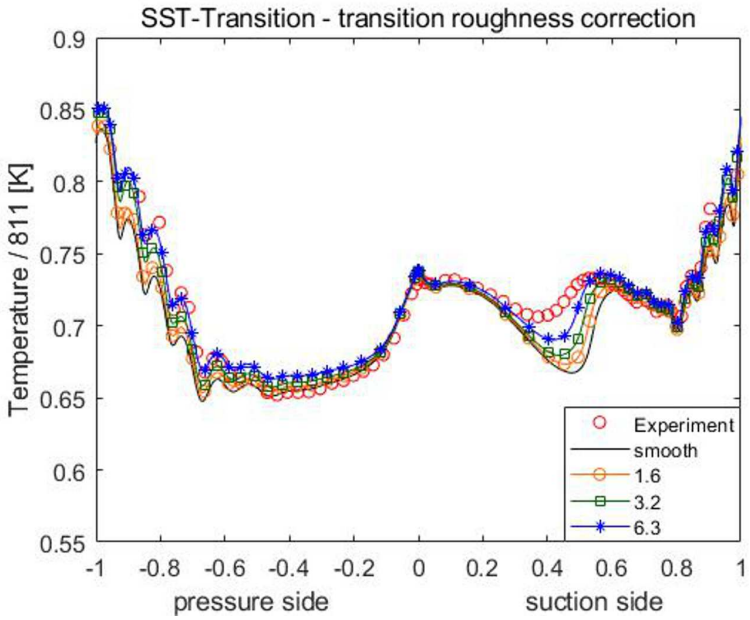

Figure 13: Temperature distribution for the SST-transition turbulence model for different wall roughness.

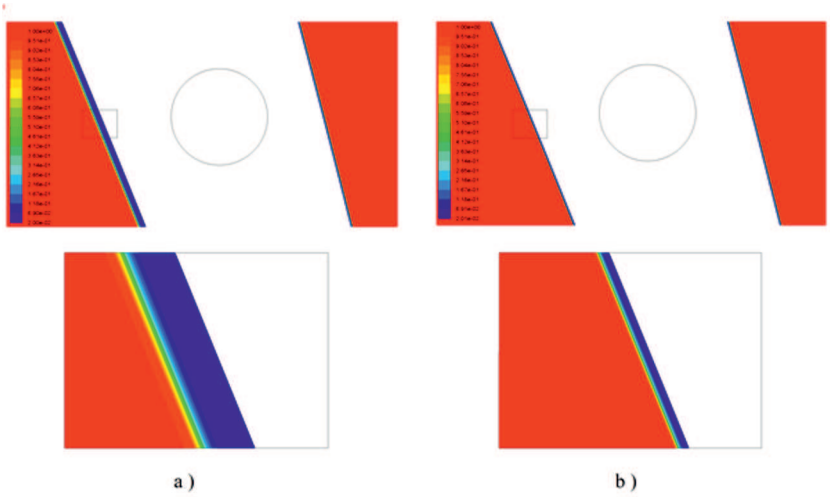

Figure 14: Intermittency distribution near the trailing edge on the pressure side: a) smooth wall, b) roughness of 6.3 μm.

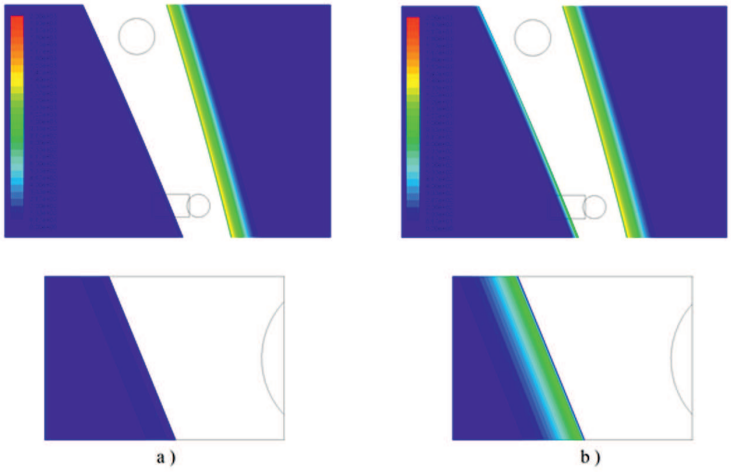

Figure 15: Turbulence kinetic energy distribution near the trailing edge for, (a) smooth wall and (b) roughness of 6.3 μm.

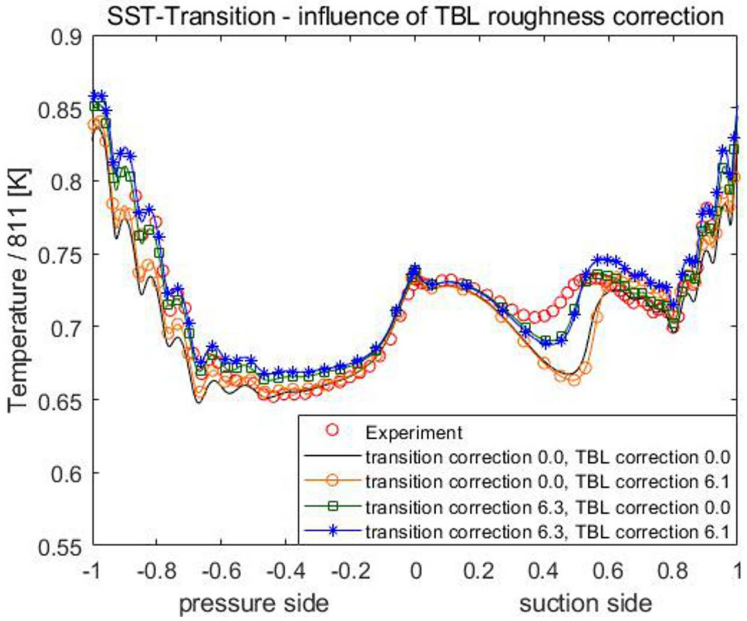

Figure 16: Temperature distribution for different roughness corrections for the intermittency transport equation and for different sand grain roughness.

The TLS significantly influenced the temperature predicted by the models, especially in the laminar zone. Moreover, the location of the transition onset depended on TLS for the γ-Re$_\theta$ SST-transition and RSM linear models, while the v^2-f showed a constant location of the turbulence initiation. For all models considered, the temperature distribution increased when TLS increased. For the v^2-f model and RSM, the results were most accurate for relatively small TLS values of around 1.524 and 3.81 mm. However, the $\gamma - \mathrm{Re}_\theta$ SST-transition was more accurate for a higher TLS value of approximately 15.24 mm. The reason of this could have been application of a production limiter in SST-transition model. The results obtained using SST-transition model without limiter showed similar trends to results evaluated by v^2-f and RSM models.

Increasing the wall roughness led to the location of the transition onset moving upstream. Moreover, for a wall roughness of 6.3 μm, a bypass transition occurred on the pressure side, which finally led to higher temperature in the solid body. The wall roughness disturbed the viscous sublayer, which led to greater heat transfer in the turbulent boundary layer.

Received in July 2017

References

[1] Badur J., Karcz M., Kucharski R., Wisniewski A., Kekana M.: *Coupled modelling of the cooling processes.* In: State of art on gas turbine research in Poland Editor T. Uhl. Cracow TU Press Kraków 2003, 19–30.

[2] Badur J., Ziółkowski P., Sławinski D., Kornet S.: *An approach for estimation of water wall degradation within pulverized-coal boilers.* Energy **92**(2015), 1, 142–152.

[3] Banaszkiewicz M.: *Numerical investigation of creep behaviour of high-temperature steam turbine components.* Trans. Inst. Fluid-Flow Mach. **124**(2012), 5–15.

[4] Banas K., Badur J.: *Influence of turbulence RANS models on heat transfer coefficients and stress distribution during thermal-FSI analysis of power turbine guide vane of helicopter turbine engine PZL-10W taking into account convergence of heat flux.* Prog. Comput. Fluid Dyn. (in press).

[5] Banas K., Badur J.: *Influence of strength differential effect on material effort of a turbine guide vane based on thermo-elasto-plastic analysis.* J. Therm. Stresses **40**(2017), 11, 1368–1385.

[6] Banaszkiewicz M.: *Online determination of transient thermal stresses in critical steam turbine components using a two-step algorithm.* J. Therm. Stresses **40**(2017), 6, 690–703.

[7] Banaszkiewicz M.: *On-line monitoring and control of thermal stresses in steam turbine rotors.* Appl. Therm. Eng. **94**(2016), 763–776.

[8] Staroselsky A., Martin T.J., Cassenti B.: *Transient thermal analysis and viscoplastic damage model for life prediction of turbine components.* J. Eng. Gas Turb. Power **137**(2015), 4, 042501.

[9] Taler J., Weglowski B., Sobota T., Jaremkiewicz M., Taler D.: *Inverse space marching method for determining temperature and stress distributions in pressure components.* In: Development in Heat Transfer, M.A.D.S. Bernardes, (Ed.) In Tech, Rijeka, 2011, ISBN: 978-953-307-569-3.

[10] Duda P.: *Inverse method for stress monitoring in pressure components of steam generators.* In Proc. 17th Int. Conf. on Structural Mechanics in Reactor Technology. Prague, 2003.

[11] Wacławczyk M., Pozorski J.: *Modeling of turbulent flow in the near-wall region using PDF method.* J. Theor. App. Mech-Pol. **41**(2003), 1, 3–18.

[12] Durbin P.A.: Pettersson Reif B.A.: *Statistical Theory and Modeling for Turbulent Flows.* John Wiley & Sons, 2011.

[13] Rumsey C.L., Pettersson Reif B.A., Gatski T.B.: *Arbitrary steady-state solutions with the K-Epsilon model.* AIAA J. **44**(2006), 7, 1586–1592.

[14] Rumsey C.L.: *Apparent transition behavior of widely-used turbulence models.* Int. J. Heat. Fluid Fl. **28**(2007), 6, 1460–1471.

[15] Bak J.G., Cho J., Lee S., Kang Y.S.: *Effects of inlet turbulence conditions and near-wall treatment methods on heat transfer prediction over gas turbine vanes.* Int. J. Aeronaut. Space **17**(2016), 1, 8–19.

[16] Pecnik R., Pieringer P., Sanz W.: *Numerical investigation of the secondary flow of a transonic turbine stage using various turbulence closures.* ASME Turbo Expo 2005: Power for Land, Sea, and Air. **6**(2005), 1185–1193.

[17] Luo J., Razinsky E. H.: *Conjugate heat transfer analysis of a cooled turbine vane using the V2F turbulence model.* J. Turbomach. **129**(2007), 4, 773–781.

[18] Menter F.R., Langtry R.B., Likki S.R., Suzen Y.B., Huang P.G., Volker S.: *A correlation based transition model using local variables Part 1: Model formulation.* J. Turbomach. **128**(2006), 3, 413–422.

[19] Lin G., Kusterer K., Ayed A.H., Bohn D., Sugimoto T.: *Conjugate heat transfer analysis of convection-cooled turbine vanes using γ-Re_θ transition model.* Int. J. Gas Turbine, Propulsion and Power Systems (JGPP) **6**(2014), 3, 9–15.

[20] Hongjun Z., Zhengping Z., Yu L., Jian Y., Songhe S.: *Conjugate heat transfer investigations of turbine vane based on transition models.* Chinese J. Aeronaut. **26**(2013), 4, 890–897.

[21] Yoshiara T., Sasaki D., Nakahashi K.: *Conjugate Heat Transfer Simulation of Cooled Turbine Blades Using Unstructured-Mesh CFD Solver.* In Proc. 49th AIAA Aerospace Sciences Meeting including the New Horizons Forum and Aerospace Exposition. Orlando, 2011.

[22] Menter F.R., Langtry R., Volker S.: *Transition modeling for general purpose CFD codes.* Flow, Turbul. Combust. **77**(2006), 1, 277–303.

[23] Hylton L.D., Mihelc M.S., Turner E.R., Nealy D.A., York R.E.: *Analytical and Experimenal Evalaluation of the Heat Transfer Distribution Over the Surfaces of Turbine Vanes.* NASA Lewis Research Center, 1983.

[24] Mendonca F., Clement J., Palfreyman D., Peck A.: *Validation of unstructured CFD modelling applied to the C3X turbine including conjugate heat transfer*. CD-adapco, London, 2011.

[25] Johansson C.: *Optimization of wall parameters using CFD*. Master Thesis, Royal Institute of Technology, 2014.

[26] Wang Z.F., Yan P.G., Tang H.F., Huang H.Y., Han W.J.: *Study of inner-cooling channel's heat transfer coefficient criteria formula of a high pressure air-cooled turbine*. J. Eng. Thermophys. **31**(2010), 2, 247–250.

[27] Sutherland W.: *The viscosity of gases and molecular force*. Philos. Mag. **5**(1893), 36, 507–531.

[28] Goldsmith A., Waterman T.E. and Hirshhorn H.J.: *Handbook of Thermophysical Properties of Solid Materials – Volume II: Alloys*. New York, USA: The Macmillian Company, 1961.

[29] ANSYS Documentation

[30] Elsner W., Warzecha P.: *Modeling of rough wall boundary layers with intermittency transport model*. TASK Quart. **14**(2010), 3, 271–282.

[31] Aupoix B.: *Wall Roughness Modelling with k-w STT Model*. In: Proc. 10th Int. ERCOFTAC Symp. on Engineering Turbulence Modeling and Measurements, 2014.

[32] Adams T., Grant C., Watson H.: *A simple algorithm to relate measured surface roughness to equivalent sand-grain roughness*. Int. J. Mech. Eng. Mechatronics **1**(2012), 1, 66–71.